Revue des Composites et des Matériaux Avancés-Journal of Composite and Advanced Materials
Vol. 36, No. 2, April, 2026, pp. 303-318
Journal homepage: http://iieta.org/journals/rcma

Dual-Functional TiO_2/HAp/Ag Nanocomposites for Enhanced Bioactivity and Antibacterial Bone Implants

Noor Sabeeh Jouda*, Abbas Fadhel Essa

Department of Physics, College of Science, Wasit University, Kut 52001, Iraq

Corresponding Author Email: noor.sabeeh1989@gmail.com

https://doi.org/10.18280/rcma.360208

Received: 4 January 2026
Revised: 11 March 2026
Accepted: 20 March 2026
Available online: 30 April 2026

Keywords:
TiO_2/HAp nanocomposite, silver-modified biomaterials, hydroxyapatite from bovine bone, bioactivity, antibacterial activity, hemocompatibility, bone repair

ABSTRACT

Titanium-based implant materials often suffer from inadequate bioactivity and postoperative infection, which remain major causes of clinical failure in bone repair. In this study, a multifunctional TiO_2/HAp/Ag nanocomposite was developed utilizing hydroxyapatite (HAp) derived from bovine bone to enhance bioactivity, antibacterial performance, and biological safety while maintaining acceptable mechanical properties. The prepared HAp exhibited a Ca/P molar ratio of 1.67 and an average crystallite size of 48.3 nm, confirming the successful formation of bone-like HAp. The TiO_2/HAp composite was subsequently modified with $AgNO_3$ and characterized by X-ray diffraction (XRD), X-ray fluorescence (XRF), Fourier transform infrared spectroscopy (FTIR), energy-dispersive X-ray spectroscopy (EDS), and field emission scanning electron microscopy (FESEM), both before and after immersion in simulated body fluid (SBF). Before immersion, the surface had a Ca/P ratio of 1.66 (Ca: 6.99 at.%, P: 4.21 at.%). After 14 days of SBF immersion, this ratio shifted to 1.53, with Ca and P contents increasing to 25.02 at.% and 16.39 at.%, respectively, indicating strong in vitro bioactivity. The Ag-modified composite also exhibited clear antibacterial activity against *Staphylococcus aureus* and *Enterococcus faecalis*, with inhibition zones of 26 and 25 mm, respectively. Hemolysis testing indicated excellent blood compatibility, with no detectable hemolytic response under the tested conditions. Mechanical evaluation yielded a Vickers hardness of 2.93 GPa, a diametral tensile strength of 18.45 MPa, and a compressive strength of 75.86 MPa. These findings demonstrate that the silver-modified TiO_2/HAp nanocomposite is a promising candidate for bone graft and implant-related biomedical applications requiring both bioactivity and antibacterial protection.

1. INTRODUCTION

The major challenge facing applications of large segmental bone grafts is achieving the optimal balance between mechanical stability and biological integrity, in addition to resisting surgery-associated bacterial infections that lead to clinical implant failure [1, 2]. Despite the widespread use of titanium and its alloys in orthopedic surgery due to their excellent mechanical properties, titanium is a bioinert material [3]. This leads to poor direct adhesion to bone tissue and the formation of fibrous tissue around the implant. To overcome these obstacles, research has focused on coating these implants with biomaterials such as hydroxyapatite (HAp) [4]. HAp, extracted from natural sources such as bovine bone, has a chemical composition and porous structure that closely resemble human bone, thus promoting osseointegration [5].

However, the problem of postoperative infection remains, necessitating the addition of antimicrobial agents to the biomaterial structure [6]. Silver nanoparticles (Ag) have emerged as a promising addition due to their superior ability to inhibit the growth of a wide range of bacteria [7]. Bacterial adhesion and biofilm formation on implant surfaces significantly impede long-term outcomes by protecting microbes from host immune responses and antibiotic therapies [8-10]. This has driven the development of multifunctional implant materials that combine structural strength with long-lasting antibacterial properties and enhanced tissue integration.

One promising strategy is the incorporation of antimicrobial agents such as silver into bioactive coatings on implant surfaces. Silver ions (Ag^+) and silver nanoparticles (AgNPs) exhibit broad-spectrum antibacterial activity by disrupting bacterial cell membranes and inhibiting cellular functions, making them attractive for preventing implant-associated infections [11-13]. When integrated into HAp, a calcium phosphate ceramic with excellent biocompatibility and chemical similarity to bone mineral, the resulting Ag- doped HAp coatings have demonstrated enhanced bactericidal performance while maintaining compatibility with osteogenic cells [14-16]. For example, multilayer coatings combining AgNPs with HAp and carbon nanotubes on Ti6Al4V substrates were found to enhance corrosion resistance and antibacterial efficacy against *Escherichia coli*, highlighting

the potential of silver-enhanced composites in dental and orthopedic applications [17]. Similarly, Ag-doped HAp/silica nanocomposite coatings significantly inhibited bacterial growth while supporting bioactivity on titanium implant surfaces in vitro [18]. While silver enhances antibacterial activity, its cytotoxic effects on mammalian cells must be carefully balanced. Studies show that controlled silver release from nanocomposite coatings can inhibit bacterial adhesion without substantially decreasing the viability of osteoblasts and other human cell lines, indicating that appropriate dosing and surface engineering can mitigate cytotoxicity concerns [19-21]. For instance, the addition of HAp to Ag-coated Ti implant surfaces enabled primary human osteoblasts to adhere and exhibit normal morphology and function, suggesting that HAp can modulate silver release and improve overall cytocompatibility [22].

Nonetheless, optimizing the distribution and concentration of silver remains critical to avoid adverse cellular responses. In addition to biological performance, mechanical properties such as hardness and compressive strength are paramount for implants intended to withstand physiological loads. Porous titanium and Ti alloy-based scaffolds are increasingly engineered to mimic natural bone mechanical characteristics, thereby reducing stress shielding and improving osseointegration [23, 24]. Mechanical surface treatments and composite coatings have been shown to enhance hardness and adhesion strength; for example, TiO_2/HAp/Ag nanocomposite coatings on Ti6Al4V substrates increased adhesion strength, hardness, and corrosion resistance compared to pure HAp coatings [25]. Such improvements in mechanical behavior are essential for ensuring durability and stable long-term function of implants under cyclic loading [26]. Reviews on advanced surface modification approaches underscore the importance of integrating antibacterial ion doping with osteogenic surface cues to promote both infection resistance and bone cell interaction [27]. Moreover, systematic analyses of metallic nanoparticle incorporation illustrate that antimicrobial enhancement can be achieved without compromising essential physical and mechanical properties [28]. Furthermore, composite designs integrating Ag/Fe co-doping into porous scaffolds have shown synergistic antibacterial effectiveness while maintaining necessary structural characteristics conducive to bone tissue regeneration [29].

Microwave-assisted synthesis methods for Ti/HAp composites also highlight the ongoing efforts to improve interfacial mechanical properties while preserving bioactivity [30]. Taken together, these studies reveal a clear trend toward developing multifunctional implant materials that address the fundamental tradeoffs between antibacterial efficacy, cytocompatibility, and mechanical performance. In this study, a 15 wt.% concentration of HAp was strategically selected based on preliminary optimization experiments. These experiments demonstrated that 15 wt.% HAp provides the optimal balance, ensuring sufficient bioactivity for osseointegration while preserving the structural integrity of the titanium dioxide (TiO_2) matrix. Compositions exceeding this limit were found to increase the brittleness of the composite, while lower concentrations failed to produce the desired biological response. Despite these advancements, a gap remains in comprehensively evaluating how silver incorporation affects antibacterial performance, cytotoxicity, and mechanical integrity within the same experimental framework, particularly for implants designed to bear significant loads. Therefore, this study aimed to develop an antibacterial agent by grafting the TiO_2–HAp substrate with silver nitrate to fabricate silver-modified porous TiO_2/HAp/Ag composites and systematically characterizes their antibacterial activity, in vitro cytotoxicity, and mechanical properties, including Vickers hardness and compressive strength, to advance multifunctional implant designs for improved clinical outcomes.

2. MATERIALS AND METHODS

The HAp nanoparticles were synthesized from a natural source, namely, the bovine bones. There were five animals whose femoral bones of the femur were used. The bones were washed thoroughly and then immersed in distilled water for six hours. All ligaments and cartilage were removed, and the bones were then re-boiled to ensure complete fat removal. A dryer was subsequently used at 75 °C for 24 hours. Calcination was carried out in an electric furnace at 700 °C for four hours. This was followed by grinding with a DAMFOX rotary center-blade crusher and sieving with an Azemoun vibratory screen to obtain HAp nanoparticles. The steps for preparing HAp from bones up to obtaining the nano-powder are illustrated in the flow diagram in Figure 1, and the shape of the bones before and after heat treatment (Supplementary Figure S1).

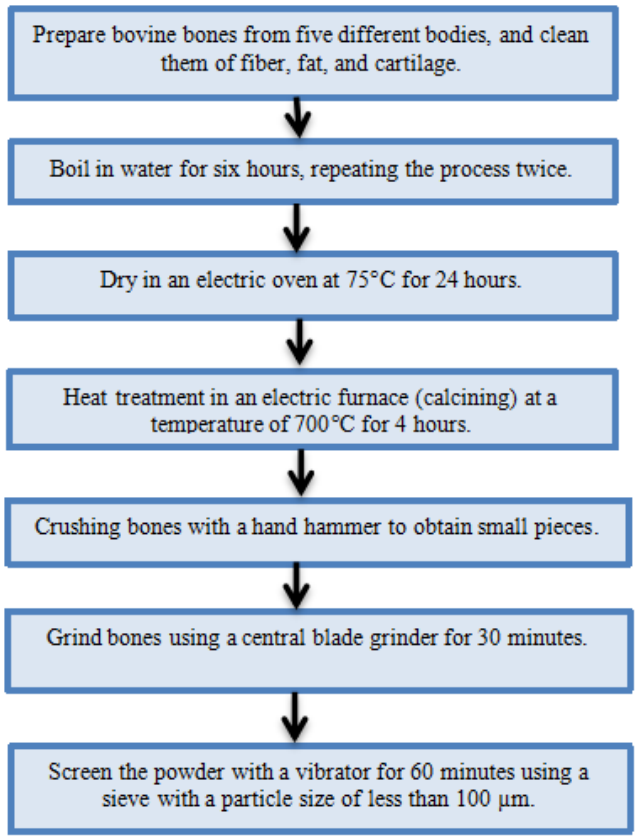

Figure 1. The diagram of the preparation of the hydroxyapatite compound from bovine bones

Commercial TiO_2, with a molecular weight of 79.6 g/mol, supplied by Nano Research USA Ltd., was used. The particle size was approximately 25 nm. Polyethylene glycol, with a molecular weight of 6000 g/mol, was employed as a binder in the preparation of the samples. It was manufactured in Germany by BASF. To prepare the ceramic composite samples, the samples were weighed according to the weight

ratio (15 wt.% HAp). Colloidal solutions of TiO_2 were then prepared and combined with specified concentrations of HAp. The powders were dissolved in ethyl alcohol by magnetic stirring for 30 minutes at 30 ℃. An ultrasonic cleaner was then used for 40 minutes at 30 ℃. Finally, filtration was performed to remove residual ethyl alcohol, yielding a TiO_2/HAp powder. The powders were dried using a dryer at 75 ℃ for 8 hours. To obtain porous samples, paraffin wax was incorporated to prepare them, which were then compressed to 3 tons using a semi-dry axial press.

The ceramic composite samples were then heat-treated at 750 ℃ for 1 hour, resulting in stable samples with adequate density. A schematic diagram of the experimental methodology can be seen in Figure 2. The preparation method and the final shape of the samples can be seen in the Supplementary Figures S2 and S3.

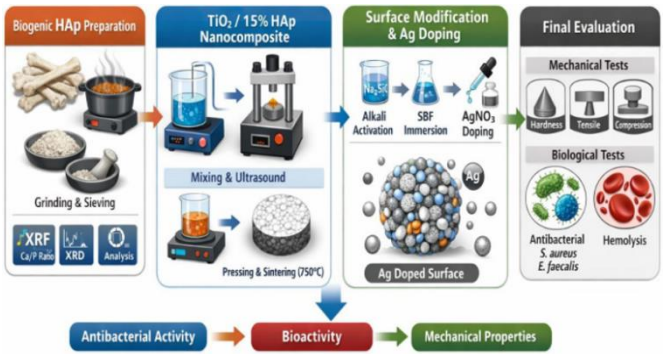

Figure 2. Schematic diagram of the experimental methodology

2.1 Alkaline surface activation using sodium silicate

Sodium silicate (Na_2SiO_3) solution was prepared using sodium silicate supplied by Thomas Baker, India, with a molar mass of 122.0632 g/mol. To prepare a 0.002 M solution, 0.0366 g of sodium silicate was dissolved in 150 mL of distilled water. The ceramic composite samples were immersed in the sodium silicate solution for seven days at 36 ℃, pH 7.4.

This process represented the alkaline pretreatment stage of the ceramic composite samples before immersion in simulated body fluid (SBF). Sodium silicate treatment of the samples is an alkaline preparatory step to enhance the surface bioactivity of the ceramic composites before the SBF immersion test. The alkaline ions activate the surface of TiO_2 by partially dissolving its less stable surface fractions and promoting hydrolysis. This results in the development of active hydroxyl groups (Ti-OH) [31]. The silicate ions in solution are then deposited over the active surface, and a protective and catalytic layer of silica hydrogel is formed. This layer, in conjunction with hydroxyl groups, provides negatively charged nucleation sites which are effective and fast in attracting calcium (Ca^{2+}) and phosphate (PO^{3-}_4) ions from SBF solution [32]. Therefore, alkaline treatment with sodium silicate significantly accelerates apatite crystal deposition on the sample surface.

2.2 In vitro bioactivity evaluation protocol

In vitro bioactivity was evaluated by immersion in SBF prepared according to the Kokubo protocol [33]. This fluid is prepared to mimic the ionic concentration of human blood plasma. The SBF solution was prepared in the laboratory by dissolving the salts listed in Table 1. The samples were incubated at 36.5 ℃ for 14 days, with solution renewal every 48 h, then rinsed with deionised water and dried at 45 ℃. The Supplementary Figure S4 illustrates a summary of the synthesis stages and the mechanism of apatite formation.

Table 1. Chemical composition and concentrations for simulated body fluid (SBF) solution preparation [33]

Reagent	Weight
NaCl	7.996 g
$NaHCO_3$	0.350 g
KCl	0.224 g
$K_2HPO_4 \cdot 3H_2O$	0.228 g
$MgCl_2 \cdot 6H_2O$	0.305 g
1.0 M HCl	11 cm^3
$CaCl_2$	0.278 g
Na_2SO_4	0.071 g
$(HOCH_2)_3CNH_2$	6.057g

2.3 Silver nitrate

Silver nitrate ($AgNO_3$) prepared by Avonchem UK, with a molecular weight of 169.87 g/mol, was used. To prepare a 0.005 M $AgNO_3$ solution, 0.0424 g of silver nitrate powder was dissolved in 50 mL of distilled water in a volumetric flask using a magnetic stirrer at 37 ℃ for 30 minutes. Ceramic composite samples were immersed in the prepared solution in an oven at 37 ℃ for 48 hours. Afterward, the solution was removed, and the samples were stored in a desiccator at 38 ℃ for 24 hours under dark conditions. Following this step, biological tests were performed by testing the samples on two different types of bacteria associated with bone implants and grafts to determine their antibacterial effectiveness, as this property is essential for biomaterials used in bone replacement.

3. MECHANICAL PROPERTY ASSESSMENT

The ceramic composite (TiO_2/HAp) was assessed in terms of mechanical properties in order to determine the intrinsic structural integrity of the material and its suitability for use as a bone substitute. This evaluation involved the measurement of indentation resistance, indirect tensile strength, and compressive strength.

3.1 Diametrical tensile strength (Brazilian test)

The diametrical tensile strength (Brazilian test) was used to determine the indirect tensile fracture resistance of the ceramic composites. Axial loading was applied along the cylindrical specimen's diametrical axis until failure. Diametrical tensile stress was determined with the help of the following equation [34]:

$$\sigma_D = \frac{2F}{\pi dD} \quad (1)$$

where,

- σ_D is the diametrical tensile strength (MPa).
- F is the applied force (N).
- D is the specimen diameter (mm).
- d is the specimen thickness (mm).

3.2 Hardness (Vickers microhardness)

A Vickers microhardness was used to determine hardness. This is an important property since it shows how the material will resist permanent plastic deformation (indentation). The Vickers test is used for ceramic specimens because it is very precise and can test the brittle nature of the material. A pyramidal diamond indenter (with an angle of 136º) was utilized with a given load over a given dwell time. The value of Vickers hardness was determined by the formula [34]:

$$H_v = \frac{1.854P}{d^2} \quad (2)$$

where,

- H_v is the Vickers hardness (GPa).
- P is the applied load (Kgf).
- d represents the average length of the long diagonals (mm).

3.3 Compressive strength

Compressive strength was determined as the maximum axial stress the ceramic composite can withstand before structural failure. This test was performed by applying a uniaxial compressive force perpendicular to the cross-sectional area of the cylindrical samples using a hydraulic press at ambient temperature. The compressive strength was calculated according to the following equation:

$$\sigma_c = \frac{F}{A} \quad (3)$$

where,

- σ_c is the compressive strength (MPa).
- F is the uniaxial compressive force (N).
- A is the original cross-sectional area (mm^2).

4. BIOLOGICAL TESTS

4.1 Biological antibacterial tests

The method of measurement was the agar well diffusion method; the Gram-positive bacteria samples used were *Staphylococcus aureus* and *Enterococcus faecalis*. For control purposes, a bacteria-free culture medium was used to ensure the purity of the medium. Dimethyl sulfoxide solvent (to ensure the presence of solvent inhibition).

4.2 Cytotoxicity test by hemolytic assay

The hemolysis technique is regarded as one of the significant techniques to determine cytotoxicity, as it is based on the evaluation of the effect of toxic agents on the integrity of cell membranes and their capability to maintain the internal elements. This test is specific to the effect of the prepared compounds on human blood cells and corpuscles in case there is some kind of contact between the compounds and the blood. It is a technique based on the capacity of the toxic materials to damage the cell membranes, which then results in leakage of the cell contents into the external environment. The amount of leaked hemoglobin is then measured and this is taken to be a measure of the degree of toxicity.

The test is performed in two phases:

First, the determination of the concentration of hemoglobin as a product of hemolysis.

Second, microscopic observation of the look of the cells and comparison with the positive control, which is a total lysis of the cells and the phosphate buffer solution (PBS).

The result is described by the hemolytic rate, along with measuring the absorbance of the hemolysis (leaked hemoglobin) using a spectrophotometer with an absorbance at 520 nm. On the other hand, the test may reflect the effectiveness of substances in their anticancer effects on cancer cells.

5. RESULTS AND DISCUSSION

5.1 X-ray fluorescence

X-ray fluorescence (XRF) was conducted on the synthesized HAp powder to determine the chemical composition of the powder, verify the weight proportion of its constituent elements, and determine the calcium -to-phosphorus ratio to compare it with the normal ratio in the bone. The analysis of the test revealed that the prepared compound is composed of major constituents of CaO (55.10 wt.%) and P_2O_5 (41.73 wt.%). The calculated Ca/P molar ratio was found to be 1.67. Details of element concentrations and elemental analysis are provided in the Supplementary (Table S1).

5.2 X-ray diffraction

X-ray diffraction (XRD) was used to determine the structural properties of HAp using a 1.54 Å copper single-wavelength spectrometer at 45 kV. The results, presented in Table 2, summarize the structural parameters of HAp and compare them with the standard data on the card (JCPDS card No. 9-432), confirming that the prepared material is HAp, as illustrated in Figure 3. The interatomic distance (d) values were calculated using Eq. (4) [35]. The average crystallite size ($C.S$) was calculated using Eq. (5) [36], yielding an average value of 48.3 nm.

Table 2. Structural properties of hydroxyapatite (hexagonal, $Ca_{10}(PO_4)_6(OH)_2$, a = b = 9.41 Å, c = 6.88 Å

2θ (deg)	Crystallite Size (*C.S*) (nm)	Miller Indices (hkl)
31.78	48.4	(211)
25.85	50.8	(002)
32.879	49.5	(300)
39.769	44.8	(310)

$$n\,\lambda = 2d\,\sin\,\theta \quad (4)$$

where,

- n is the order of reflection (integer).
- λ is the X-ray wavelength (Å).
- d is the interatomic spacing (Å).
- θ is the diffraction angle (degrees).

$$C.S = K\lambda / \beta\,COS\theta \quad (5)$$

where,

- $C.S$ is the crystallite size (nm).
- K is the Scherrer constant.
- λ is the X-ray wavelength (Å).
- β is the full width at half maximum (FWHM) of the peak (radians).
- θ is the Bragg angle (degrees).

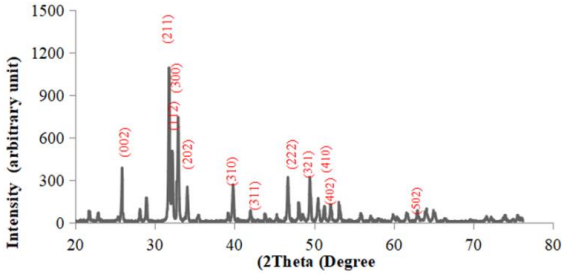

Figure 3. X-ray diffraction (XRD) spectrum of Hydroxyapatite Nano composite, $Ca_{10}(PO_4)_6(OH)_2$

5.3 Fourier transform infrared spectroscopy

Fourier transform infrared spectroscopy (FTIR) spectra were obtained for all composite ceramic samples (TiO_2/HAp) before and after immersion in SBF, as shown in Table 3 and Figure 4. FTIR spectra in the wavenumber range 400-4000 cm^{-1} were used to identify the chemical bonds and functional groups, which exhibited standard bands assigned to different vibrations. The peaks in the range 3640-3570 cm^{-1} indicate the presence of a hydroxyl group (OH^-). Conversely, the peaks at 1025-1090 cm^{-1} indicate phosphate bonds, suggesting the presence of calcium phosphate phases such as HAp. Spectral analysis of the ceramic composite TiO_2/HAp revealed fifteen distinct peaks, representing various chemical bonds and functional vibrations. The main peaks of HAp in this sample are located at 1050.96, 1090.328, 634.80, 602.723 cm^{-1}. The peaks representing free calcium phosphate are observed at 1631.981, 962.876 cm^{-1}, while the peak 1458.128 cm^{-1} represents di-calcium phosphate. The details of the FTIR analysis of pure HAp are presented in the Supplementary (Table S2 and Figure S5).

When comparing the spectral analysis of the same sample after immersion in SBF for 14 days, a significant reduction in the number of peaks was observed. Consequently, certain chemical bonds disappeared, including the peaks associated with free calcium phosphate. However, one peak indicating di-calcium phosphate remained, along with three prominent peaks representing HAp, as detailed in Table 4 and Figure 5.

Table 3. Fourier transform infrared spectroscopy (FTIR) analysis of the ceramic composite (TiO_2/15% HAp) before immersion in simulated body fluid (SBF)

Peak No.	Absorption Peak (cm^{-1})	Bond Type	Vibration Mode	Intensity
1	3428.93	OH	Stretching	Strong
2	2924.37	C-H	Stretching	Medium
3	2853.86	C-H	Stretching	Medium
4	2014.04	C-O	Overtone combination	Weak
5	1740.63	C=O	Stretching	Strong
6	1631.98	C-O-H	Bending	Medium
7	1458.12	C-O	Bending	Medium
8	1413.10	C-O	Bending	Weak
9	1384.94	C-H	Bending	Weak
10	1090.77	P=O	Stretching	Medium
11	1050.96	P=O	Stretching	Strong
12	962.87	P-O	Stretching	Weak
13	634.83	P-O	Bending	Weak
14	602.72	P-O	Bending	Weak
15	572.26	P-O	Bending	Weak

Table 4. Fourier transform infrared spectroscopy (FTIR) analysis of the ceramic composite (TiO_2/15% HAp), after immersion in simulated body fluid (SBF)

Peak No.	Absorption Peak (cm^{-1})	Bond Type	Vibration Mode	Intensity
1	3434.22	OH	Stretching	Strong
2	2925.50	C-H	Stretching	Medium
3	2854.50	C-H	Stretching	Medium
4	1631.54	C-O-H	Bending	Medium
5	1458.16	C-O	Bending	Weak
6	1091.26	P=O	Stretching	Medium
7	1052.23	P=O	Stretching	Strong
8	602.79	P-O	Bending	Weak
9	572.16	P-O	Bending	Weak

Table 5. Surface chemical composition and Ca/P molar ratio of TiO_2/HAp composite before and after immersion in simulated body fluid (SBF)

Surface Chemical State	Ca/P Molar Ratio	P (at.%)	Ca (at.%)	Ti (at.%)	Condition
(TiO_2/HAp)	1.66	4.21	6.99	48.6	Pre-immersion
Bone-like Apatite Formation	1.53	16.39	25.02	41.2	Post-immersion

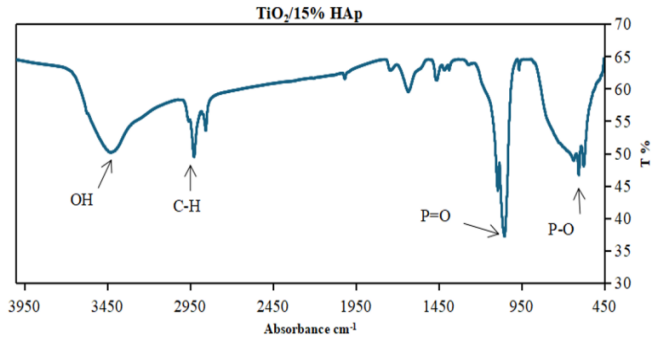

Figure 4. Fourier transform infrared spectroscopy (FTIR) for the ceramic composite (TiO_2-15% HAp), pre-simulated body fluid (SBF)

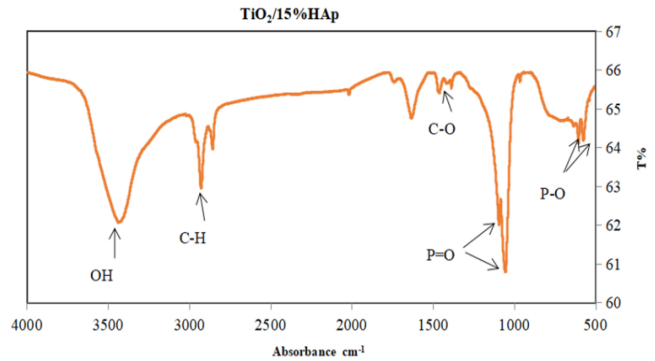

Figure 5. Fourier transform infrared spectroscopy (FTIR) for the ceramic composite (TiO_2-15% HAp), post-simulated body fluid (SBF) for 14 days

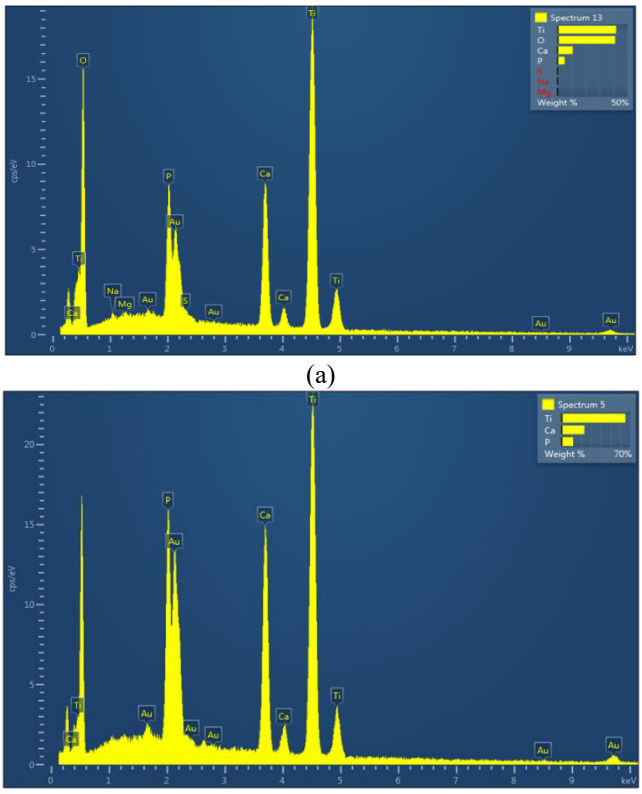

(a)

(b)

Figure 6. Energy-dispersive X-ray spectroscopy (EDS) spectra of the TiO_2/HAp composite (a) before immersion in simulated body fluid (SBF) and (b) after immersion in SBF

5.4 The energy-dispersive X-ray spectroscopy

Energy-dispersive X-ray spectroscopy (EDS) results for as-prepared TiO_2/HAp ceramic composite before and after immersion in SBF are presented in Table 5 and Figure 6. Analysis of the pre-immersion sample revealed a calcium-to-phosphorus (Ca/P) molar ratio of 1.66, which corresponds to the optimal value for HAp. Post-immersion spectral analysis indicated that the phosphorus-to-calcium ratios doubled compared to initial levels. This increase suggests the formation of a dense apatite layer, demonstrating the high bioactivity of the titanium surface within the 14-day immersion period.

5.5 Field effect scanning electron microscope

Field emission scanning electron microscopy (FESEM) analysis was performed on the (TiO_2/HAp) ceramic composite samples to evaluate their surface morphology before immersion in SBF. The samples exhibited a particle size of around 50 nm, characterized by tightly packed grains with minimal aggregation. Furthermore, a distribution of pores between the grains was also observed. The samples were heat-treated at 750 ℃ to enhance the grain density while maintaining sufficient porosity. This porous structure is designed to promote bone cohesion, fluid flow, and ion movement, thereby facilitating the development of a natural apatite layer.

The heat treatment regime also resulted in particle fusion and cohesion, reducing inter-particle distances and achieving a suitable density while maintaining porosity. Figures 7 and 8 show FESEM images of the ceramic composite samples (TiO_2/HAp) before and after immersion in SBF for 14 days. The images reveal small, white, scattered grains on the surface, which are deposits resulting from the accumulation of calcium and phosphate ions after immersion in the SBF.

5.6 Mechanical performance evaluation

The mechanical characteristics of the ceramic composite TiO_2/HAp were determined after heat treatment at 750 ℃. H_v was determined as a quantitative parameter of the resistance of the material to permanent plastic deformation under concentrated stress. Upon the application of the test and calculation of the results based on Eq. (2), it was found that the composite has a H_v value of 2.93 GPa. In order to determine the fracture resistance of the material to tensile stresses, a Brazilian tensile test was conducted [37-39]. Calculations from Eq. (1) showed a tensile strength of 18.45 MPa. Moreover, the compressive strength was found to be 75.86 MPa after the application of Eq. (3).

5.7 Antibacterial test evaluation

The biological activity of the prepared ceramic composites, composed of TiO_2 replaced with varying weight percentages of HAp (15 wt.% HAp) and saturated with 0.005% $AgNO_3$, was evaluated after immersion in a SBF for 14 days. The result, presented in Table 6, demonstrates that TiO_2 and HAp control samples exhibited no antibacterial activity due to their biologically inert nature. Furthermore, Figure 9 demonstrated that the ceramic composite samples exhibit antimicrobial activity against Gram-positive bacteria (*Staphylococcus aureus* and *Enterococcus faecalis*), with inhibition zone diameters ranging from 25 to 25 mm (Figure 9).

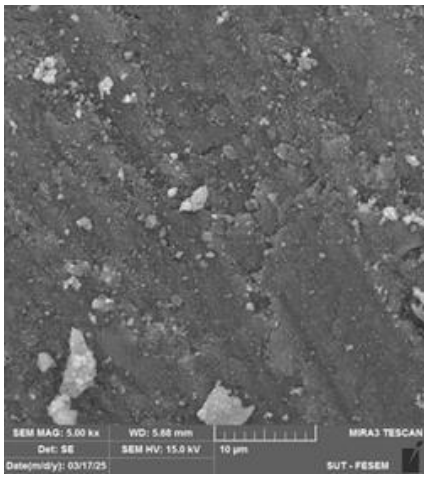

(a)

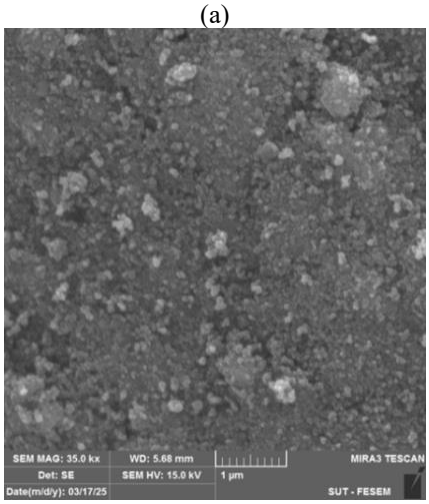

(b)

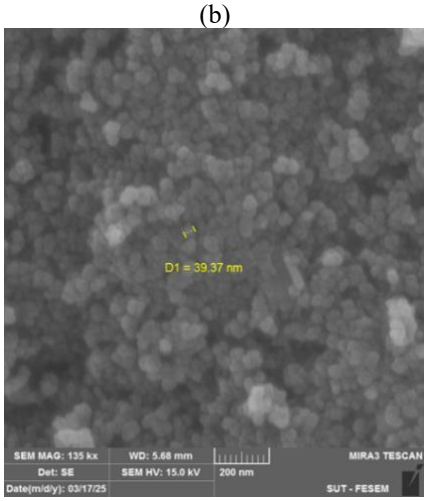

(c)

Figure 7. Field emission scanning electron microscopy (FESEM) images of the TiO_2/HAp ceramic composite, pre-immersion in SBF at different magnifications (see Figure S6)

Table 6. Antibacterial activity of (TiO_2/HAp/Ag) compounds against Gram-positive bacteria based on inhibition zone diameters

Sample	$AgNO_3$ Concentration (M)	Activity-Inhibition (mm)	
		E.faecalis	***S.aureus***
TiO_2/15% HAp	0.0 (Control)	2	1
TiO_2/15% HAp	0.005	26	25

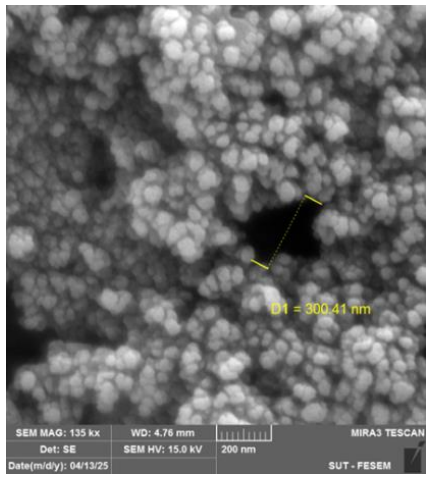

(a)

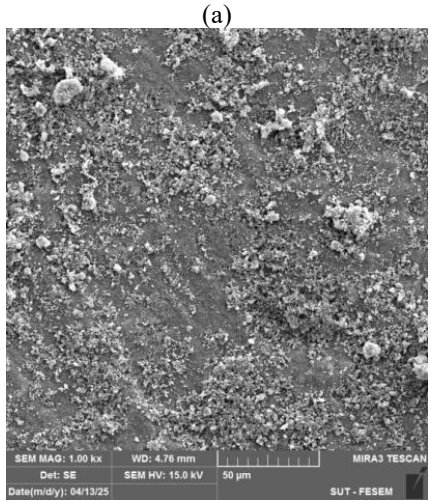

(b)

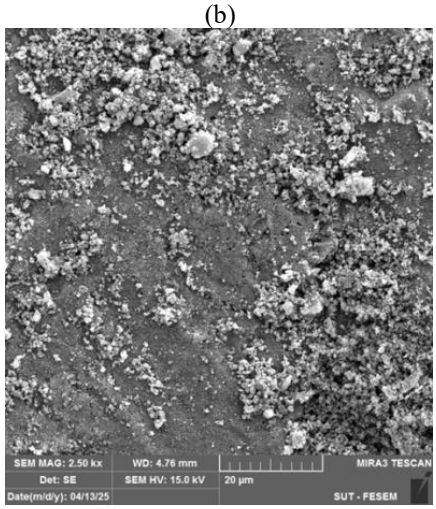

(c)

Figure 8. Field emission scanning electron microscopy (FESEM) images of the TiO_2/HAp ceramic composite, post-immersion in SBF at different magnifications (see Figure S7)

5.8 Cytotoxicity test by hemolysis assay

A hemolysis assay was performed to evaluate the compatibility of the synthesized bioceramic composites (TiO_2/HAp/Ag) with blood, as shown in Table 7, which represents the percentage of human red blood cell hemolysis induced by these composites. The symbol (N.H) indicates no hemolysis, confirming the absence of cytotoxicity. This was further verified by observing the color change in the test tubes containing the material and a suspension of purified human red

blood cells, compared to the positive control sample ($^{+}$C). After two hours of incubation, neither sample showed hemolysis, as shown in Figure 10(a) and Table 8, which presents the change in absorbance values at a wavelength of 540 nm. This is evident from the lack of the dark red color in the upper liquid, whereas the positive control sample exhibited intense redness as a result of total cell hemolysis. The Blood assay is shown in Figure 10(b). Microscopic analysis of blood samples was performed; the red blood cells did not exhibit toxic or hemolytic effects from the compounds, and their biconcave shape was maintained, and no evidence of membrane rupture or shrinkage was detected.

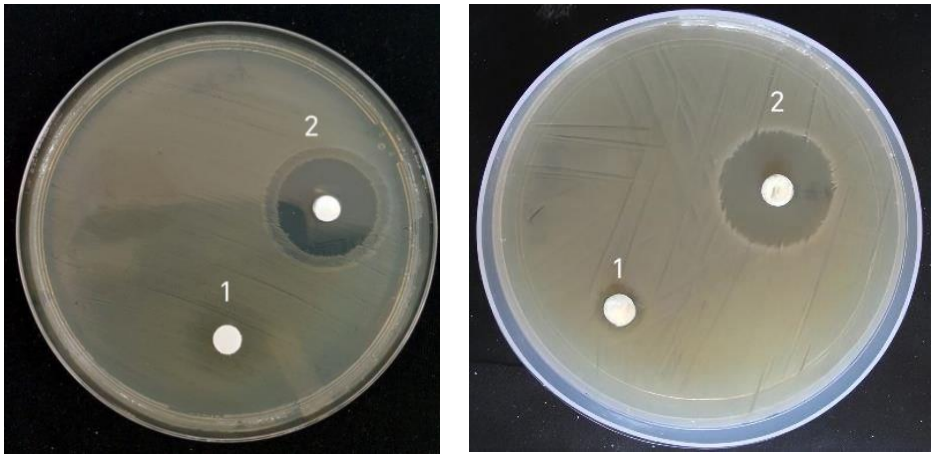

(a) (b)

Figure 9. Antibacterial activity of TiO_2/HAp/Ag ceramic composite against: (a) *Staphylococcus aureus* and (b) *Enterococcus faecalis*

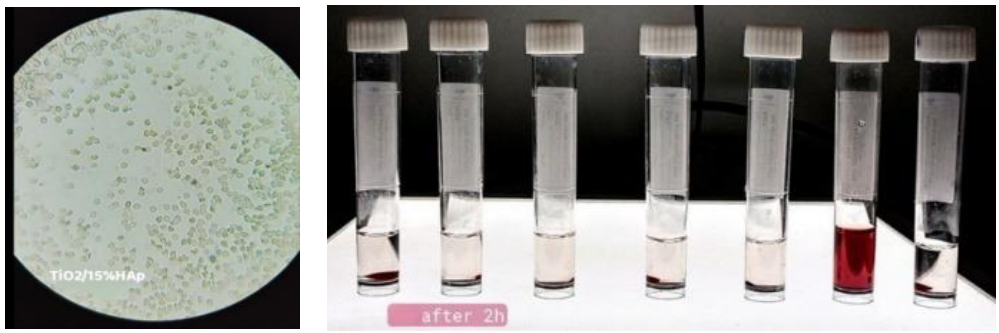

(a) (b)

Figure 10. Hemolysis assay and microscopic evaluation of red blood cells: (a) Optical micrographs of cells incubated with TiO_2/HAp/Ag for 2 hours, showing maintained morphology; (b) Qualitative hemolysis results in test tubes containing the chemical additive and purified blood cell solution, after incubation for 2 hours

Table 7. Percentage of human red blood cell hemolysis (hemolytic rate) induced by the TiO_2/HAp (A) and TiO_2/HAp /Ag (B) composites

Concentrations	Hemolysis Rate of Samples HR%		+ Control	- Control
	A	B		
1/10	N.H	N.H	100%	N.H
1/100	N.H	N.H	100%	N.H
1/1000	N.H	N.H	100%	N.H
1/10000	N.H	N.H	100%	N.H
1/100000	N.H	N.H	100%	N.H

Table 8. Absorbance values of the TiO_2/HAp/Ag composite at 540 nm across varying concentrations

Concentrations	Absorption
1/10	0.6
1/100	0.6
1/1000	0.6
1/10000	0.6
1/100000	0.6
Positive control	1.25 nm
Negative control	0.6 nm

Note: Absorbance is unitless; values for positive and negative controls are reported as measured

6. DISCUSSION

6.1 Structural properties of HAp (X-ray fluorescence and X-ray diffraction)

XRF analysis demonstrated that the HAp prepared from bovine bones exhibited high purity. The Ca/P molar ratio was Ca/P = 1.67, consistent with reference values and the standard ratios of minerals found in natural bone [39]. The results confirmed the presence of naturally occurring elements such as Na and Mg, which cannot be obtained through the synthetic preparation of HAp. UV Magnesium is essential for stimulating cell division and tissue growth, while sodium directly contributes to ion exchange. Maintaining a standard balance of minerals is crucial for ensuring the biological stability of implants when placed in biological systems.

XRD results of the prepared HAp powder confirmed its high degree of crystallinity, and the diffraction peaks obtained corresponded to the chemical formula of HAp ($Ca_{10}(PO_4)_6(OH)_2$). This indicates the success of the heat treatment in removing the organic components present in the bovine bones.

6.2 Chemical bonding and stability analysis (Fourier transform infrared spectroscopy)

FTIR spectroscopy results confirmed the successful incorporation of HAp within the TiO_2 matrix. The clear appearance of phosphate (PO_4^{3-}) and hydroxyl (OH^-) group peaks after sintering directly reflects the thermal stability of the nanocomposite. The presence of 15 vibrational peaks before immersion in the SBF indicates a complex chemical environment among the composite components.

The decrease in the number of peaks to nine vibrational peaks after 14 days of immersion in SBF suggests chemical reactions resulting from the formation of a new apatite layer on the material surface. The detection of dicalcium phases in addition to HAp is a strategic advantage, as these phases contribute to accelerating ion exchange upon contact with body fluids. This early chemical reaction paves the way for the formation of the bio-calcium-deficient hydroxyapatite (CDHA) layer.

6.3 Interpretation of energy-dispersive X-ray spectroscopy and bioactivity mechanisms

The Ca/P ratio after immersion suggests that the material possesses a higher surface energy, which enhances bone conduction. This allows the material to dissolve slowly, enabling normal bone growth within it. The release of calcium ions effectively stimulates osteoblasts. The stable Ca/P molar ratio of 1.53, along with the spherical shape observed by FESEM, confirms the formation of CDHA. This phase resembles the natural mineral found in mammalian bones, indicating the high bioactivity of the treated titanium surface and its potential to form strong chemical bonds with bone tissue in the future, making it a possible application as a graft for treating bone defects.

The rapid apatite layer formation can be attributed to the synergistic effect of alkaline treatment with sodium silicate and the use of high-purity, biologically derived HAp containing Na, Mg, and other elements not present in commercially available HAp. Furthermore, the silicate treatment significantly contributed to the formation of silanol (Si-OH) groups on the titanium surface, which act as active sites for crystal nucleation. This gives the surface a negative charge that attracts calcium ions (Ca^{2+}) from the SBF solution. The accumulation of positive charges also attracts phosphate ions (PO_4^{3-}), thus stimulating the deposition of a CDHA layer [37]. The shift in the Ca/P ratio to 1.53 indicates a high degree of ion exchange, which increases the surface energy and thermodynamic solubility of the formed layer. This, in turn, enhances osteoconductivity by creating a more dynamic interface for protein uptake, a prerequisite for successful osteointegration in clinical applications [38].

6.4 Mechanical properties discussion

The orthopedic composites should be evaluated mechanically to determine their suitability. The high gain in penetration resistance is explained by the interconnected internal strengthening mechanism. The phase composition can explain the growth in tensile strength. The quantity of HAp employed, the sintering temperature (750 °C), and the optimum dispersion of the HAp particles all helped to enhance the fracture resistance of the material by enabling a crack deflection mechanism.

This process directs cracks on the microscopic scale on a zigzag course, which consumes more fracture energy and minimizes the chances of catastrophic failure. Compressive strength, which is an important mechanical property in determining the aptitude of a material to be used as a bone implant, was measured. This value is used to show the compressive strength against the axial forces of the material that can resist structural failure. Load-bearing bone applications need to be stable in the long term [40].

The value is in line with the outcomes of other mechanical tests and puts the material in the range of strength needed in bone implants. This is within the high range of cancellous bone (2-50 MPa) and close to the lower range of cortical bone (100-230 MPa) [41]. The mechanical properties of the current study were compared with those of normal bone and reference studies in Table 9. This minimizes the chance of the so-called stress shielding effect, which may cause the surrounding bone to resorb, hence demonstrating the mechanical efficiency of the material in the biological setting.

Table 9. Comparison of the mechanical properties of the current study with the physiological ranges of cortical and cancellous bone

Ref.	Vickers Hardness (GPa)	Tensile Strength (MPa)	Compressive Strength (MPa)	Material
---	2.93	18.45	75.86	Current Study (TiO_2/HAp/Ag)
[42]	0.39-0.60	10-30	100-230	Human Cortical Bone
[42]	---	1-5	2-50	Human Cancellous Bone
[43]	2.1-3.8	8.5-15.0	65.4-95.2	TiO_2/HAp Bioceramic
[44]	2.5-3.2	---	72.0-88.5	TiO_2/nHAp Composite

6.5 Antibacterial mechanisms and synergistic effects

This experiment sought to examine how the structural and compositional characteristics of the composites influenced the antimicrobial activity of the composites. The formation of transparent halos around wells on Mueller-Hinton plates suggests the potential of the composites to inhibit bacterial growth, with wider halos indicating stronger antibacterial activity. The three ceramic composite components exhibit a significant synergistic effect in this antibacterial action. The silver nitrate particles facilitate the formation of Ag^+, which can react with the bacterial cellular components, e.g., proteins and DNA, thereby interfering with the essential processes in the cells and causing their death.

TiO_2 also has photo-catalytic and oxidative characteristics, which generate reactive oxygen species (ROS), which disrupt the cell wall of bacteria and enhance membrane permeability [45]. HAp is a biocompatible, porous material that enhances surface adhesion, providing a larger surface area for the gradual release of Ag^+ and thereby sustaining the antibacterial effect over time [46].

The improved functional performance of the TiO_2/HAp/Ag ceramic composite is primarily due to its regular porous structure and the balanced distribution of AgNPs within interconnected pores. These pores act as reservoirs, allowing the diffusion of biological fluids and ions. This behavior enables the stable release of Ag^+ rather than a rapid and sudden release. The surface porosity creates a controlled pattern of Ag^+ release, thus maintaining an effective concentration for a longer period.

Furthermore, immersion in SBF for 14 days resulted in the formation of a CDHA layer, which further stabilizes the ceramic composite surface. This layer enhances bioactivity because CDHA tends to be more reactive than HAp, acting as a diffusion barrier that regulates ion exchange. This ensures sustained antibacterial activity. The dual-functional performance of this composite, which combines high biological activity and a chemical composition similar to the mineral phase of natural bone, in addition to a porous structure that contributes to bone conduction and antibacterial activity, gives this composite high efficiency that makes it suitable for bone grafting applications [47].

6.6 Hemocompatibility and toxicity discussion

The absence of hemolysis indicates the absence of cytotoxicity. Microscopic analysis was performed to establish that the compounds did not influence cell morphology. This high compatibility with blood is explained by the synergistic physicochemical interaction of the constituents. HAp creates a non-toxic, stable and inert surface, which limits direct contact with red blood cells [48-50].

7. CONCLUSIONS

This study successfully prepared a high-purity, biogenic HAp nanocomposite from sustainable natural sources. It also developed a ceramic composite (TiO_2/HAp/Ag) with enhanced functional properties. This composite combines rapid bone fusion, resistance to bacterial infection, and mechanical properties compatible with cancellous bone, while exhibiting no toxicity to red blood cells.

The synthesized ceramic composite possesses promising properties, making it suitable for medical applications as a bone graft that stimulates autologous bone tissue healing through a precise biomimetic mechanism.

REFERENCES

[1] Zhang, H., Wu, Z., Wang, Z., Yan, X., Duan, X., Sun, H. (2025). Advanced surface modification techniques for titanium implants: A review of osteogenic and antibacterial strategies. Frontiers in Bioengineering and Biotechnology, 13: 1549439. https://doi.org/10.3389/fbioe.2025.1549439

[2] Medina, E.L., Vaca-González, J.J., Aperador, W., Ramtani, S., Falentin-Daudre, C., Garzón-Alvarado, D. (2025). Review of advanced coatings for metallic implants: A study/proposal on yttria-stabilized zirconia and silver-doped hydroxyapatite: Medina, vaca-gonzález, aperador, ramtani, falentin-daudre, and garzón-alvarado. JOM, 77(7): 5345-5361. https://doi.org/10.1007/s11837-025-07345-8

[3] Zhao, X., You, L., Wang, T., Zhang, X., Li, Z., et al. (2020). Enhanced osseointegration of titanium implants by surface modification with silicon-doped titania nanotubes. International Journal of Nanomedicine, 15: 8583-8594. https://doi.org/10.2147/IJN.S270311

[4] Li, J., Zheng, Y., Yu, Z., Kankala, R.K., Lin, Q., Shi, J., Chen, C., Luo, K., Chen, A., Zhong, Q. (2023). Surface-modified titanium and titanium-based alloys for improved osteogenesis: A critical review. Bioactive Materials, 10(1): e23779. https://doi.org/10.1016/j.heliyon.2023.e23779

[5] Paital, S.R., Dahotre, N.B. (2009). Calcium phosphate coatings for bio-implant applications: Materials, performance factors, and methodologies. Materials Science and Engineering, R: Reports, 66(1-3): 1-70. https://doi.org/10.1016/j.mser.2009.05.001

[6] Odusote, J.K., Danyuo, Y., Baruwa, A.D., Azeez, A.A. (2019). Synthesis and characterization of hydroxyapatite from bovine bone for production of dental implants. Journal of Applied Biomaterials & Functional Materials, 17(2): 2280800019836829. https://doi.org/10.1177/2280800019836829

[7] Akay, S., Yaghmur, A. (2024). Recent advances in antibacterial coatings to combat orthopedic implant-associated infections. Molecules, 29(5): 1172. https://doi.org/10.3390/molecules29051172

[8] Karataş, H., Eker, F., Akdaşçi, E., Bechelany, M., Karav, S. (2026). Silver nanoparticles in antibacterial research: Mechanisms, applications, and emerging perspectives. International Journal of Molecular Sciences, 27(2): 927. https://doi.org/10.3390/ijms27020927

[9] Salaie, R.N., Besinis, A., Le, H., Tredwin, C., Handy, R.D. (2020). The biocompatibility of silver and nanohydroxyapatite coatings on titanium dental implants with human primary osteoblast cells. Materials Science and Engineering: C, 107: 110210. https://doi.org/10.1016/j.msec.2019.110210

[10] Radhi, N.S., Hamzah, S., Jasim, T.A., Al-Khafaji, Z., Falah, M., Al-Aloosi, W.M. (2025). Surface engineering of titanium via micro-arc oxidation with hydroxyapatite/nano-silver composite coatings: In vitro and in vivo biological performance evaluation. Advanced Engineering Letters, 4(3): 112-125.

https://doi.org/10.46793/adeletters.2025.4.3.4
[11] Iconaru, S.L., Predoi, D., Ciobanu, C.S., Motelica-Heino, M., Guegan, R., Bleotu, C. (2022). Development of silver doped hydroxyapatite thin films for biomedical applications. Coatings, 12(3): 341. https://doi.org/10.3390/coatings12030341
[12] Sevencan, A., Doyuk, E.K., Köse, N. (2020). Silver ion doped hydroxyapatite-coated titanium pins prevent bacterial colonization. Joint Diseases and Related Surgery, 32(1): 35-41. https://doi.org/10.5606/ehc.2021.79357
[13] Ji, X., Qian, X., Luo, G., Yang, W., Huang, W., et al. (2025). Engineered macrophage nanoparticles enhance microwave ablation efficacy in osteosarcoma via targeting the CD47-SIRPα Axis: A novel Biomimetic immunotherapeutic approach. Bioactive Materials, 47: 248-265. https://doi.org/10.1016/j.bioactmat.2025.01.012
[14] Liao, Z., Li, J., Su, Y., Miao, F., Zhang, X., et al. (2023). Antibacterial hydroxyapatite coatings on titanium dental implants. Frontiers of Materials Science, 17(1): 230628. https://doi.org/10.1007/s11706-023-0628-x
[15] Haugen, H.J., Makhtari, S., Ahmadi, S., Hussain, B. (2022). The antibacterial and cytotoxic effects of silver nanoparticles coated titanium implants: A narrative review. Materials, 15(14): 5025. https://doi.org/10.3390/ma15145025
[16] Pang, S., Wu, D., Yang, H., Kamutzki, F., Kurreck, J., Gurlo, A., Hanaor, D.A. (2023). Enhanced mechanical performance and bioactivity in strontium/copper co-substituted diopside scaffolds. Biomaterials Advances, 145: 213230. https://doi.org/10.1016/j.bioadv.2022.213230
[17] Mishchenko, O., Volchykhina, K., Maksymov, D., Manukhina, O., Pogorielov, M., Pavlenko, M., Iatsunskyi, I. (2025). Advanced strategies for enhancing the biocompatibility and antibacterial properties of implantable structures. Materials, 18(4): 822. https://doi.org/10.3390/ma18040822
[18] Diez-Escudero, A., Andersson, B., Carlsson, E., Recker, B., Link, H., Järhult, J.D., Hailer, N.P. (2022). 3D-printed porous Ti6Al4V alloys with silver coating combine osteocompatibility and antimicrobial properties. Biomaterials Advances, 133: 112629. https://doi.org/10.1016/j.msec.2021.112629
[19] Dewi, N., Gartika, M., Gustiono, D., Kurnia, D., Cahyanto, A. (2025). Antimicrobial and antibiofilm properties of hydroxyapatite/nano-hydroxyapatite in preventing dental caries: A systematic review. European Journal of Dentistry, 19(3): 563-579. https://doi.org/10.1055/s-0045-1802568
[20] Morimoto, T., Hirata, H., Eto, S., Hashimoto, A., Kii, S., et al. (2022). Development of silver-containing hydroxyapatite-coated antimicrobial implants for orthopaedic and spinal surgery. Medicina, 58(4): 519. https://doi.org/10.3390/medicina58040519
[21] Wątroba, M., Bednarczyk, W., Szewczyk, P.K., Kawałko, J., Mech, K., et al. (2023). In vitro cytocompatibility and antibacterial studies on biodegradable Zn alloys supplemented by a critical assessment of direct contact cytotoxicity assay. Journal of Biomedical Materials Research Part B: Applied Biomaterials, 111(2): 241-260. https://doi.org/10.1002/jbm.b.35147
[22] Yadav, M.K., Akshay, Y., Naga, A.Y., Praveenkumar, K., et al. (2025). Processing and development of porous titanium for biomedical applications: A comprehensive review. Journal of Manufacturing and Materials Processing, 9(12): 401. https://doi.org/10.3390/jmmp9120401
[23] Kedia, S., Checker, R., Sandur, S.K., Nilaya, J.P. (2023). Picosecond laser-induced hybrid groove structures on Ti-6Al-4V bio-alloy to accelerate osseointegration. Journal of Biomedical Materials Research Part B: Applied Biomaterials, 111(10): 1775-1784. https://doi.org/10.1002/jbm.b.35284
[24] dos Reis-Neta, G.R., Ricomini-Filho, A.P., Martorano-Fernandes, L., Vargas-Moreno, V.F., Cury, A.A.D.B., Marcello-Machado, R.M. (2024). Effect of hydroxyapatite nanoparticles coating of titanium surface on biofilm adhesion: An in vitro study. Archives of Oral Biology, 164: 105986. https://doi.org/10.1016/j.archoralbio.2024.105986
[25] Marin, E., Lanzutti, A. (2023). Biomedical applications of titanium alloys: A comprehensive review. Materials, 17(1): 114. https://doi.org/10.3390/ma17010114
[26] Cao, B., Lin, J., Tan, J., Li, J., Ran, Z., Deng, L., Hao, Y. (2023). 3D-printed vascularized biofunctional scaffold for bone regeneration. International Journal of Bioprinting, 9(3): 702. https://doi.org/10.18063/ijb.702
[27] Movva, A.K., Sohn, M.O., McCloskey, C.P., Tennyson, J.M., Mitra, K., Adams, S.B., Anastasio, A.T. (2026). Next-generation biomaterials: Advanced coatings and smart interfaces for implant technology: A narrative review. Coatings, 16(1): 87. https://doi.org/10.3390/coatings16010087
[28] Tian, B., Chen, W., Dong, Y., Marymont, J.V., et al. (2016). Silver nanoparticle-loaded hydroxyapatite coating: Structure, antibacterial properties, and capacity for osteogenic induction in vitro. RSC Advances, 6(11): 8549-8562. https://doi.org/10.1039/C5RA25391H
[29] Hashimoto, A., Miyamoto, H., Kobatake, T., Nakashima, T., et al. (2020). The combination of silver-containing hydroxyapatite coating and vancomycin has a synergistic antibacterial effect on methicillin-resistant Staphylococcus aureus biofilm formation. Bone & Joint Research, 9(5): 211-218. https://doi.org/10.1302/2046-3758.95.BJR-2019-0326.R1
[30] Hamza, S., Radhi, N.S., Sahi, N.M. (2021). Study the antibacterial activity of hydroxyapatite-nano silver coating on titanium substrate. Journal of Physics: Conference Series, 1973(1): 012107. https://doi.org/10.1088/1742-6596/1973/1/012107
[31] Takadama, H., Kim, H.M., Kokubo, T., Nakamura, T. (2001). TEM-EDX study of mechanism of bonelike apatite formation on bioactive titanium metal in simulated body fluid. Journal of Biomedical Materials Research: An Official Journal of the Society for Biomaterials, the Japanese Society for Biomaterials, and the Australian Society for Biomaterials and the Korean Society for Biomaterials, 57(3): 441-448. https://doi.org/10.1002/1097-4636(20011205)57:3%3C441::AID-JBM1187%3E3.0.CO;2-B
[32] Hench, L.L. (1998). Bioceramics. Journal of the American Ceramic Society, 81(7): 1705-1728. https://doi.org/10.1111/j.1151-2916.1998.tb02540.x
[33] Kokubo, T., Kushitani, H., Sakka, S., Kitsugi, T.,

Yamamuro, T. (1990). Solutions able to reproduce in vivo surface-structure changes in bioactive glass-ceramic A-W3. Journal of Biomedical Materials Research, 24(6): 721-734. https://doi.org/10.1002/jbm.820240607
[34] Jouda, N.S., Essa, A.F. (2022). Preparation and study of the physical and mechanical properties for hydroxyapatite-titanium and zirconia nanoparticle. AIP Conference Proceedings, 2394(1): 090025. https://doi.org/10.1063/5.0121960
[35] Band, Y.B., Avishai, Y. (2013). Quantum Mechanics with Applications to Nanotechnology and Information Science. Academic Press, New York.
[36] Monshi, A., Foroughi, M.R., Monshi, M.R. (2012). Modified Scherrer equation to estimate more accurately nano-crystallite size using XRD. World Journal of Nano Science and Engineering, 2(3): 154-160. https://doi.org/10.4236/wjnse.2012.23020
[37] LeGeros, R. Z. (1991). Calcium phosphates in oral biology and medicine. Monographs in Oral Science, 15: 1-201.
[38] Jouda, N.S., Essa, A.F. (2021). Preparation and study of the structural, physical and mechanical properties of hydroxyapatite nanocomposite. Materials Today: Proceedings, 47: 5999-6005. https://doi.org/10.1016/j.matpr.2021.04.550
[39] Sycińska-Dziarnowska, M., Ziąbka, M., Cholewa-Kowalska, K., Klesiewicz, K., Spagnuolo, G., Lindauer, S.J., Park, H.S., Woźniak, K. (2025). Antibacterial and antibiofilm activity of layers enriched with silver nanoparticles on orthodontic microimplants. Journal of Functional Biomaterials, 16(1): 78. https://doi.org/10.3390/jfb16030078
[40] Burchard, R., Graw, J.A., Soost, C., Schmitt, J. (2023). Stress shielding effect after total hip arthroplasty varies between combinations of stem design and stiffness—A comparing biomechanical finite element analysis. International Orthopaedics, 47(8): 1981-1987. https://doi.org/10.1007/s00264-023-05825-7
[41] Essa, A.F., Jouda, N.S. (2022). Preparation and study of the structural properties of the hydroxyapatite–Titania and zirconia nanostructures system. AIP Conference Proceedings, 2450(1): 020004. https://doi.org/10.1063/5.0096412
[42] Ratner, B.D., Hoffman, A.S., Schoen, F.J., Lemons, J.E. (2020). Biomaterials Science: An Introduction to Materials in Medicine (4th ed.). Academic Press, New York.
[43] Dhiflaoui, H., Ben Salem, S., Salah, M., Dabaki, Y., et al. (2023). Influence of TiO_2 on the microstructure, mechanical properties and corrosion resistance of hydroxyapatite HaP + TiO_2 nanocomposites deposited using spray pyrolysis. Coatings, 13(7): 1283. https://doi.org/10.3390/coatings13071283
[44] Rahmani, R., Rosenberg, M., Ivask, A., Kollo, L. (2019). Comparison of mechanical and antibacterial properties of TiO2/Ag ceramics and Ti6Al4V-TiO_2/Ag composite materials using combined SLM-SPS techniques. Metals, 9(8): 874. https://doi.org/10.3390/met9080874
[45] Shkarina, S., Shkarin, R., Weinhardt, V., Melnik, E., et al. (2018). 3D biodegradable scaffolds of polycaprolactone with silicate-containing hydroxyapatite microparticles for bone tissue engineering: High-resolution tomography and in vitro study. Scientific Reports, 8(1): 8907. https://doi.org/10.1038/s41598-018-27097-7
[46] Trzaskowska, M., Vivcharenko, V., Benko, A., Franus, W., et al. (2024). Biocompatible nanocomposite hydroxyapatite-based granules with increased specific surface area and bioresorbability for bone regenerative medicine applications. Scientific Reports, 14(1): 28137. https://doi.org/10.1038/s41598-024-79822-0
[47] Bamal, D., Singh, A., Chaudhary, G., Kumar, M., et al. (2021). Silver nanoparticles biosynthesis, characterization, antimicrobial activities, applications, cytotoxicity and safety issues: An updated review. Nanomaterials, 11(8): 2086. https://doi.org/10.3390/nano11082086
[48] Huang, Y., Song, G., Chang, X., Wang, Z., et al. (2018). Nanostructured Ag+-substituted fluorhydroxyapatite-TiO_2 coatings for enhanced bactericidal effects and osteoinductivity of Ti for biomedical applications. International Journal of Nanomedicine, 13: 2665-2684. https://doi.org/10.2147/IJN.S162558
[49] Kiran, A.S.K., Kumar, T.S., Sanghavi, R., Doble, M., Ramakrishna, S. (2018). Antibacterial and bioactive surface modifications of titanium implants by PCL/TiO_2 nanocomposite coatings. Nanomaterials, 8(10): 860. https://doi.org/10.3390/nano8100860
[50] Sæbø, I.P., Bjørås, M., Franzyk, H., Helgesen, E., Booth, J.A. (2023). Optimization of the hemolysis assay for the assessment of cytotoxicity. International Journal of Molecular Sciences, 24(3): 2914. https://doi.org/10.3390/ijms2403291

NOMENCLATURE

A	Original cross-sectional area (mm^2)
D	Specimen diameter (mm)
n	The order of reflection (integer)
$C.S$	The crystallite size (nm)
H_v	Vickers hardness (GPa)
P	Applied load (for hardness/ strength) (Kgf)
d	Average diagonal length of indentation (mm)
Ca/P	Calcium-to-phosphorus molar ratio
IZ	Inhibition zone diameter (mm)
σ_c	Compressive strength (MPa)
σ_D	Tensile strength (MPa)

Greek symbols

Θ	Bragg diffraction angle (Degree)
β	Full width at half maximum (FWHM), Radian
λ	X-ray wavelength, nm

Abbreviations

wt.%	Weight percentage
at.%	Atomic percentage
HAp	Hydroxyapatite
TiO_2	Titanium dioxide
$AgNO_3$	Silver nitrate
SBF	Simulated body fluid
XRD	X-ray diffraction
FESEM	Field emission scanning electron microscopy
FTIR	Fourier transform infrared spectroscopy
EDS	Energy-dispersive X-ray spectroscopy

APPENDIX

Figure S1. (A) The shape of the bones before heat treatment, (B) The shape of the bones after heat treatment, (C) Hydroxyapatite (HAp) powder prepared in the laboratory

Figure S2. Schematic diagram of the experimental methodology, including the extraction of biogenic HAp, compound synthesis, biorecruitment protocols, and mechanical properties

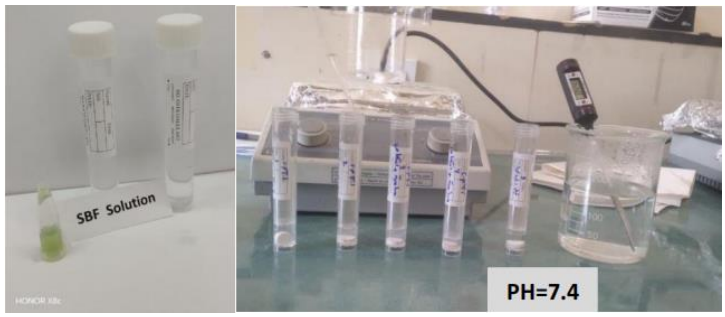

Figure S3. Steps for preparing the ceramic composite (TiO_2/HAp)

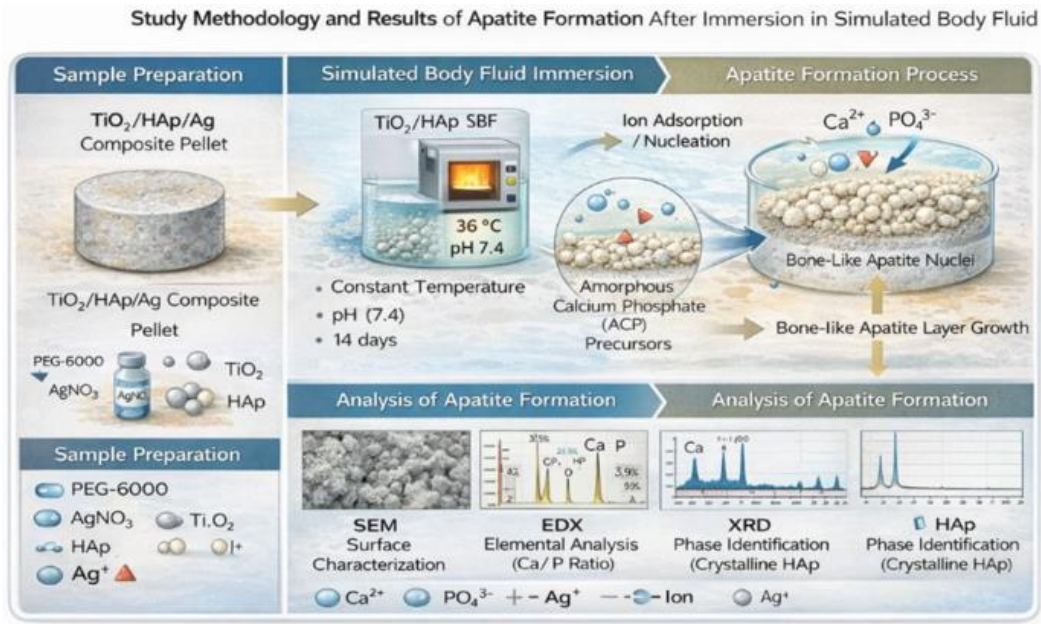

Figure S4. A summary of the synthesis stages and the mechanism of apatite formation

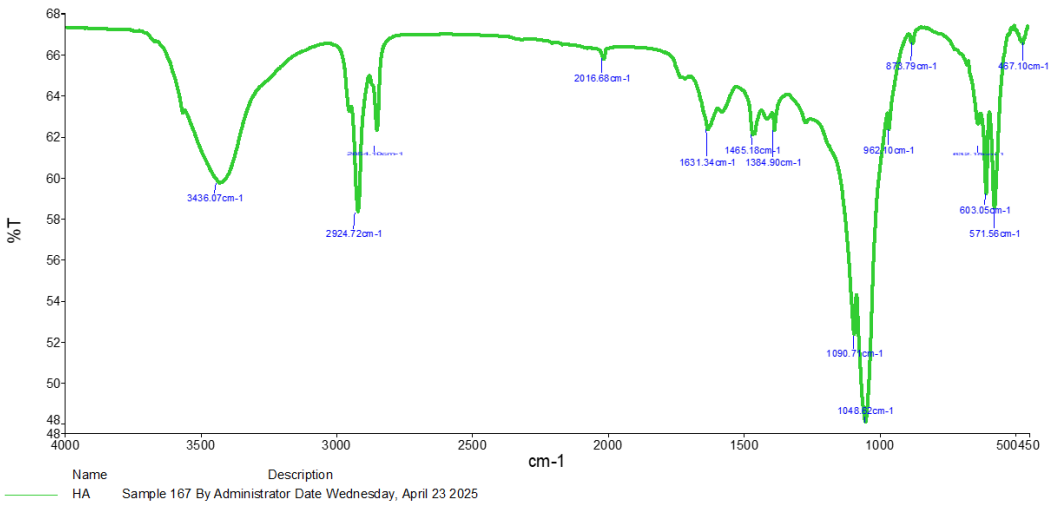

Figure S5. Fourier transform infrared spectroscopy (FTIR) for the pure HAp

Table S1. X-ray fluorescence (XRF) results showing the percentages of Hydroxyapatite powder elements

Symbol	Element	Concentration (wt.%)
MgO	Magnesium	3.06
P_2O_5	Phosphorus	41.73
Cl	Chlorine	0.06
CaO	Calcium	55.10
Ba	Barium	0.03
ZnO	Zinc	0.01

Others*	Trace elements	0.01
Total		100.00

Note: *Others include trace amounts of Al, Si, S, K,Na,Zr and Ti. **The molar ratio was derived from XRF oxide weights by converting CaO and P_2O_5 to their respective molar quantities (n_{Ca} and n_P), resulting in a stoichiometric ratio of 1.67

Table S2. Fourier transform infrared spectroscopy (FTIR) analysis of pure HAp

Peak Number	X (cm^{-1})	Y (%T)
1	3436.07	59.80
2	2924.72	58.39
3	2854.10	62.40
4	2016.68	65.89
5	1631.34	62.42
6	1465.18	62.17
7	1384.90	62.40
8	1090.71	52.36
9	1048.62	48.04
10	962.10	62.44
11	873.79	66.67
12	632.15	62.70
13	603.05	59.28
14	571.56	58.57
15	467.10	66.68

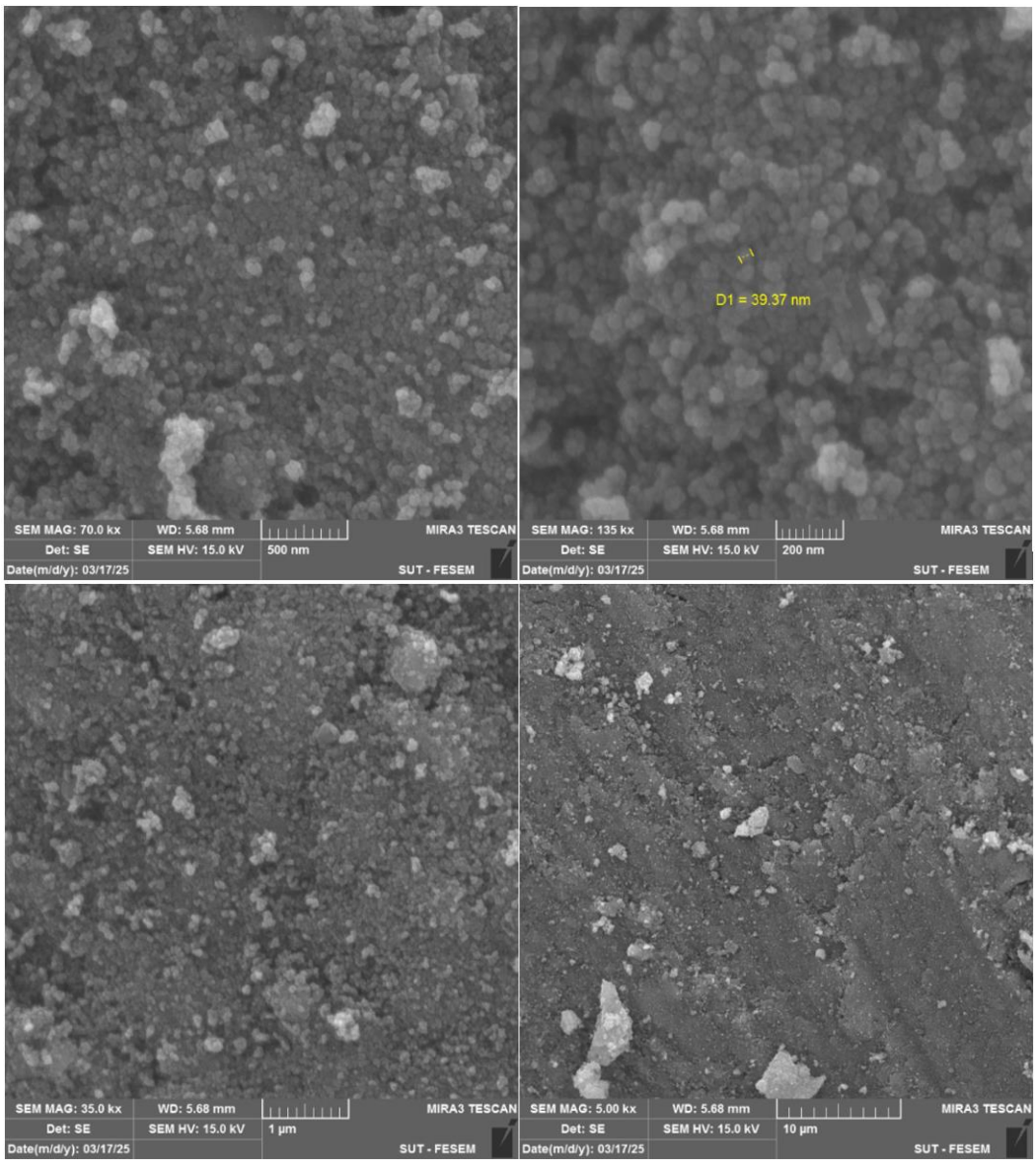

Figure S6. Field emission scanning electron microscopy (FESEM) images of the TiO_2/HAp ceramic composite before immersion in the simulated body fluid (SBF)

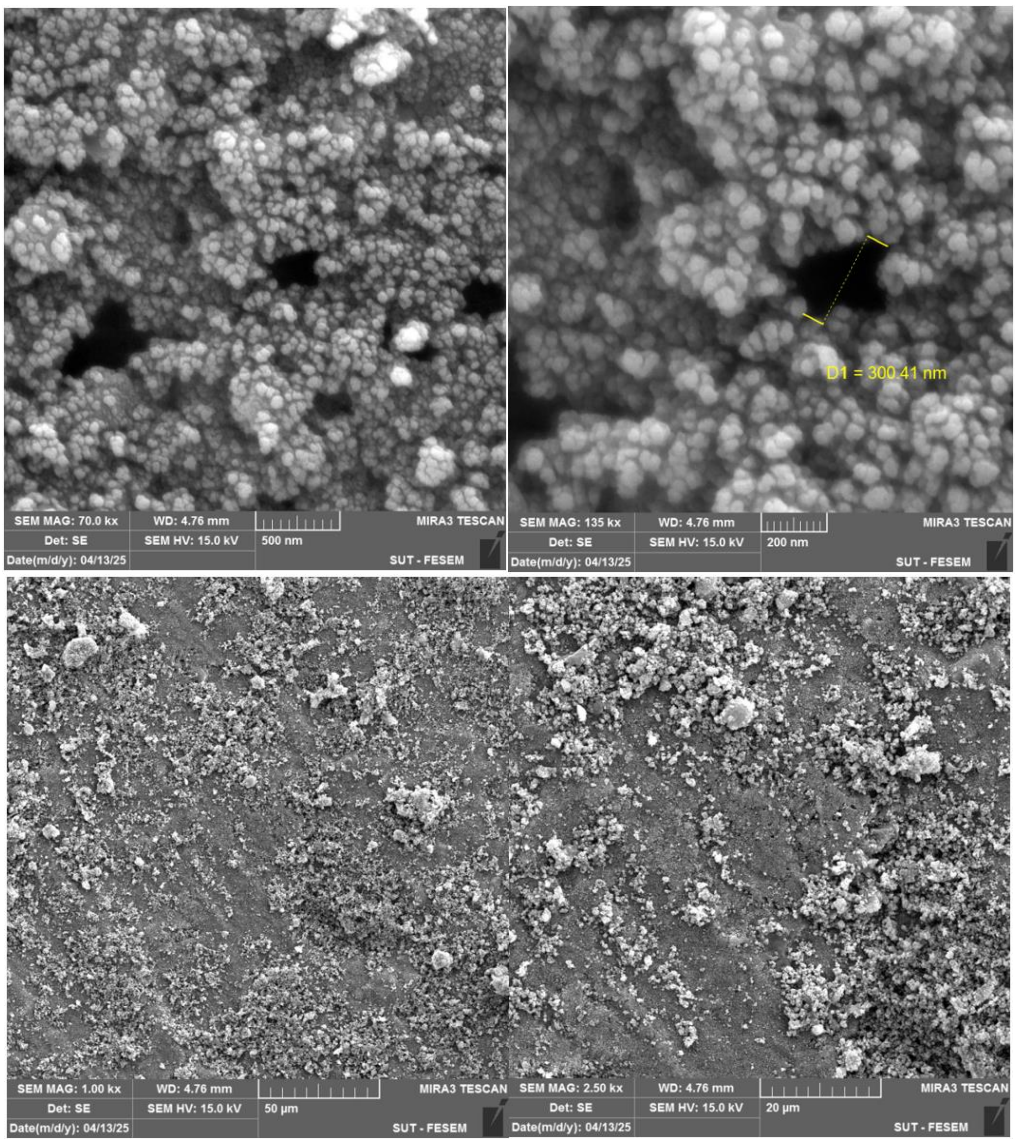

Figure S7. Field emission scanning electron microscopy (FESEM) images of the TiO_2/HAp ceramic composite after immersion in the simulated body fluid (SBF)